33RD CONGRESS
OF THE INTERNATIONAL COUNCIL
OF THE AERONAUTICAL SCIENCES
STOCKHOLM, SWEDEN, 4–9 SEPTEMBER, 2022

ICAS 2022 SWEDEN

ASSESSMENT OF FAILURE UNDER LONGITUDINAL COMPRESSION OF UNIDIRECTIONAL COMPOSITES WITH IN-PLANE FIBER MISALIGNMENT

Alfredo R. de Faria[1]

[1]Instituto Tecnológico de Aeronáutica, São José dos Campos, SP 12228-615, Brazil

Abstract

This work employs a micromechanical theory and kinematic relationships to describe the displacement field in individual unidirectional composite plies. The technique relies on an incremental approach where the misalignment angle of fibers is the main variable in the analysis. Upon convergence at a certain loading level, stresses and strains are evaluated in the fibers and matrix using micromechanics, and a specific failure criterion is applied. The Ramberg-Osgood relations are used to correct degraded mechanical properties of the resin in the nonlinear regime. The Hashin-Rotem failure criterion and experimental data obtained in the literature are used to validate the technique. It is observed that the numerical and experimental results obtained correlate well.

Keywords: UD composites, longitudinal compressive failure, damage mechanics, finite elements

1. Introduction

Unlike failure criteria for metallic materials, the composites failure criteria are rarely able to encompass the diversity of failure mechanisms involved. The inherent anisotropy of composites results in a complex behavior, particularly in the interface fiber-matrix. Thus, over time, researchers have proposed and developed different failure criteria, from the simplest to the most sophisticated ones. For instance, maximum stress criterion, maximum strain criterion, Tsai-Wu [1], Hashin-Rotem [2] and Dávila-Camanho [3] are very popular failure criteria. However, even with sound theories validated, certification of composite materials for aerospace applications still relies on testing due to the complex nature and variability of the material. According FAA requirement [4], the structural component must be subject to the ultimate load and must withstand that load for up to three seconds. Practice and commercial information involving important aircraft manufacturers show that, under certain circumstances, a composite structural component fails before the expected ultimate load. Failure under longitudinal compression in laminates with fiber misalignment, microbuckling or kink band formation (Fig. 1) may be the cause for these early failures, since these are often disregarded in the design and analysis phases. Aircraft structural components that may be prone to failure under longitudinal compression are wing upper panels, fuselage panels, rudders and control surfaces alike.

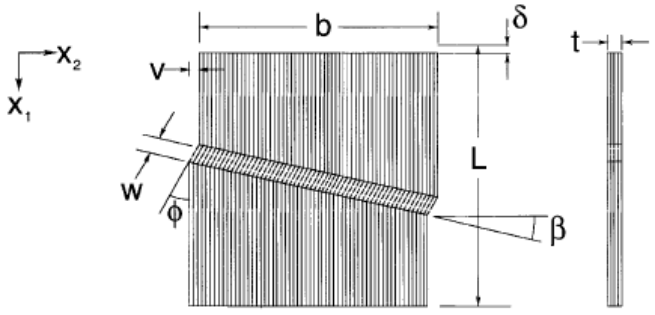

Figure 1 – Kink band parameters [11].

Rosen [5] was the first researcher to model fiber microbuckling. Two buckling modes were assessed: matrix under shear and matrix under compression. Matrix yielding was considered in order to model kink behavior in the investigations of Argon [6] and Budiansky [7]. Argon used a rigid perfectly plastic constitutive model, whereas Budiansky used an elastic perfectly plastic constitutive model. Budiansky and Fleck [8] proposed a generalized approach using the Ramberg-Osgood equation to define the matrix stress × strain relation and concluded that the elastic perfectly plastic constitutive model provided acceptable estimations. The importance of fiber misalignment was discussed by Wilhelmsson *et al.* [9], whereas aspects related to fiber curvature were addressed by Pimenta *et al.* [10].

In order to conduct research on failure mechanisms in composites experimental tests must be done and theoretical criteria must be proposed. Vogler and Kyriakides [11] investigated initiation and growth of kink bands in AS4/PEEK composites. The experimental procedure was carried out under compressive loading followed by incremental shear loading. Observation of kink band initiation was related to reduction in the shear stiffness and consequent drop in shear stress. As additional transverse displacement takes place, the kink band width increases. Vogler and Kyriakides found the parameters shown in Fig. 1: the band width "w" was around 25 times the fiber diameter, the kink band inclination "β" of 12º remained constant throughout loading, and angle "ϕ" reached approximately 26º as the kink band evolved.

Another representative test was made by Lee and Waas [12]. In their work, the mechanical properties of the fibers, fiber volume fraction and nonuniform fiber fabrication were considered in order to understand the failure mechanisms. Vinyl ester resin, glass fibers and carbon fibers with fiber volume fraction of 10% up to 60% were investigated. The finite element simulation for the carbon fiber with 4º misalignment and fiber volume fraction of 30%-40% agreed with experimental results.

Vogler *et al.* [13] used 2D and 3D numerical models to validate kink band initiation and growth in filament composites. The 2D model was idealized considering alternating layers of fibers and matrix consistent with the fiber volume fraction. On the other hand, the 3D model was idealized considering circular fibers distributed in a hexagonal arrangement over the matrix, where fiber spacing was consistent with the fiber volume fraction. The main conclusions were: (i) rupture is governed by the interaction of the nonlinear shear with small fiber misalignments, (ii) prediction of the kink band inclination requires matrix models that accurately capture its sensibility to pressure and its elasticity, (iii) kink band start off from a local imperfection, (iv) the elasto-plastic solid used to simulate the matrix was appropriate to predict failure initiation, and (v) the overall characteristics of the kink band in both 2D and 3D were similar. In Bogetti *et al.* [14], a nonlinear tridimensional model of maximum progressive deformation, based on laminate analyses, was used to predict 12 test cases representing failure envelopes and isotropic, unidirectional and multidirectional stress × strain curves. The analytical models developed by Chou *et al.* [15] and Bogetti *et al.* [16] were used to predict the effective stress × strain response of the laminate. The nonlinear lamina constitutive relations (stress × strain) along each one of the lamina principal directions were defined according to the Ramberg-Osgood [17] equation. The authors state that one significant limitation of their approach, based on the maximum strain failure criterion, is that it may be unable to model and predict damage propagation in composite laminates due to its reduced post-failure capabilities.

In experimental and theoretical investigations, Matsuo and Kageyama [18] addressed composite thermoplastics. The study assumed that kink band rupture is produced by rupture under transverse traction, as well as shear and plastic deformation. In Fig. 2 the symbol σ^{∞} represents the external compressive stress, ϕ_0 is the initial misalignment fiber angle, γ is the additional shear strain, τ is the shear stress, σ_T is the transverse traction stress on the kink band region and β is the kink band angle. In the work of Matsuo and Kageyama the predicted resistance to compression depends on the transverse elastic modulus under traction, the shear modulus in the fiber direction, parameters related to the Ramberg-Osgood curve, the initial fiber angle misalignment, two arbitrary points on the experimental shear stress × shear strain curve, the ultimate stress of transverse traction and the ultimate shear stress of the linear/nonlinear region. The initial fiber misalignment angle of the experimental sample, before compression, was 3º and the carbon fiber volume fraction was around 50%. It was deemed that the proposed criterion accurately represents experimental data and

combined stresses. Moreover, it may be applicable to assess compressive strength of other composite materials, including multiaxial laminates.

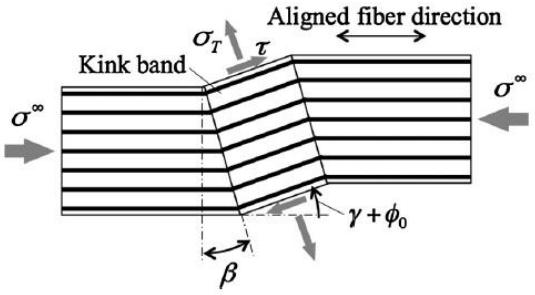

Figure 2 – Stresses in the kink band [18].

Recently, Vignoli *et al.* [19] analyzed several micromechanical models to estimate failure in laminates. The in-plane traction, compression and shear failure criteria analytically estimated were compared to experimental data available in the literature. For instance, regarding longitudinal compressive strength, 8 micromechanical models, including a new model to estimate misalignment effects, were compared against 61 experiments. The paper emphasizes that longitudinal compressive strength is highly influenced by fibers misalignment, inducing a large array of failure mechanisms, and that the material in-plane shear response is highly nonlinear. Concerning shear strength, the model of Zhang and Waas [20] presented a better estimate for failure initiation, whereas the model of Huang [21] presented a better estimate for rupture under shear.

Based on the literature review, one may identify contributions in different and diverse topics. The importance of the fiber volume fraction and the characteristics of the resin material is very clear in all investigations. Besides, one observes that most investigations assume uniaxial loadings (axial or shear), usually disregarding multiaxial loadings. Therefore, the proposal of this work includes relations between micromechanics and macromechanics, obtained through the knowledge of deformations in the plane due to the multiaxial loading of the laminate. The Ramberg-Osgood curve is used to adjust for the resin material in the nonlinear regime. An innovative aspect of the proposed approach is that it exclusively considers the fiber angle misalignment increment as analysis variable to determine convergence. Once convergence is achieved, the fiber and matrix stresses are computed, and a specific failure criterion may be assessed. Particularly, the Hashin-Rotem failure criterion and experimental data provided by Matsuo [18] are used to validate the proposed technique.

2. Analysis Technique

Figure 3 illustrates a ply in the kink band region. Three reference systems are used: (i) the structural reference system XY, (ii) the principal reference system of the ply 12, and (iii) the reference system of misalignment xy. The conventional ply angle is ϕ_0, where the subscript '0' has been added to emphasize that this is a constant value. The initial misalignment angle (unloaded condition) is θ_0. The principal stresses of the lamina σ_1, σ_2, τ_{12} are also shown.

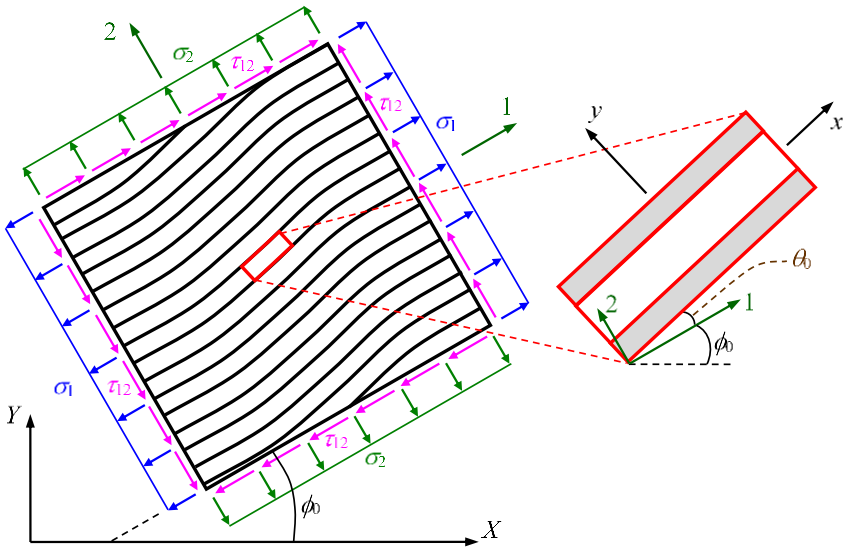

Figure 3 – Representative volume in the kink-band region.

Once loading starts the misalignment angle evolves to $\theta + \theta_0$ and Fig. 4 shows the deformed configuration.

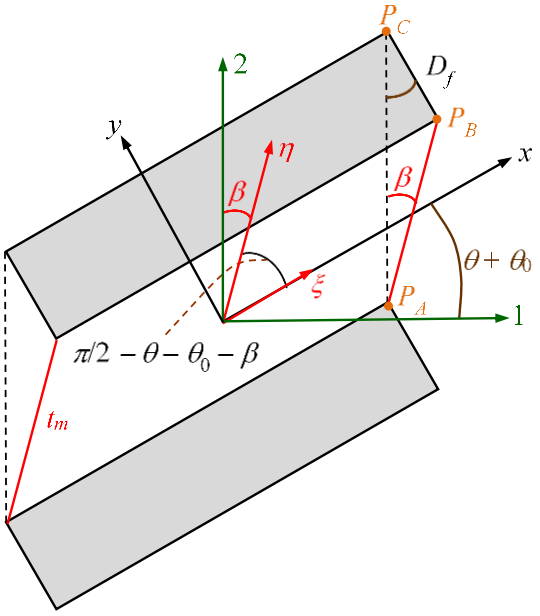

Figure 4 – Deformed configuration.

Triangle $P_AP_BP_C$ allows one to write the simple geometric relationship

$$D_f \sin(\theta + \theta_0) = t_m \sin\beta \tag{1}$$

A similar relationship can be written referring to the undeformed configuration,

$$D_f \sin\theta_0 = t_m \sin\beta_0 \tag{2}$$

The position of an arbitrary point in the xy reference system before and after deformation is initially determined using the non-orthogonal coordinates ξ and η indicated in Fig. 4, where the ξ axis is parallel to x and the η axis is parallel to P_AP_B. Before deformation the coordinates of a point are x_0, y_0 and, after deformation, x, y, with

$$x_0 = \xi + \eta \sin(\theta_0 + \beta_0) \qquad y_0 = \eta \cos(\theta_0 + \beta_0) \tag{3}$$

$$x = \xi + \eta \sin(\theta + \theta_0 + \beta) \qquad y = \eta \cos(\theta + \theta_0 + \beta) \tag{4}$$

Transformation to the 12 reference system yields,

$$x_{120} = x_0 \cos\theta_0 - y_0 \sin\theta_0 \qquad y_{120} = x_0 \sin\theta_0 + y_0 \cos\theta_0 \tag{5}$$

$$x_{12} = x \cos(\theta + \theta_0) - y \sin(\theta + \theta_0) \qquad y_{12} = x \sin(\theta + \theta_0) + y \cos(\theta + \theta_0) \tag{6}$$

Equations (3) and (5) can be combined to yield,

$$\begin{Bmatrix} \xi \\ \eta \end{Bmatrix} = \begin{bmatrix} \cos(\theta_0 + \beta_0) & -\sin(\theta_0 + \beta_0) \\ 0 & 1 \end{bmatrix} \frac{1}{\cos(\theta_0 + \beta_0)} \begin{bmatrix} \cos\theta_0 & \sin\theta_0 \\ -\sin\theta_0 & \cos\theta_0 \end{bmatrix} \begin{Bmatrix} x_{120} \\ y_{120} \end{Bmatrix} = \frac{1}{\cos(\theta_0 + \beta_0)} \begin{bmatrix} \cos\beta_0 & -\sin\beta_0 \\ -\sin\theta_0 & \cos\theta_0 \end{bmatrix} \begin{Bmatrix} x_{120} \\ y_{120} \end{Bmatrix} \tag{7}$$

Similarly, Eqs. (4) and (6) can be combined to yield

$$\begin{Bmatrix} x_{12} \\ y_{12} \end{Bmatrix} = \begin{bmatrix} \cos(\theta + \theta_0) & -\sin(\theta + \theta_0) \\ \sin(\theta + \theta_0) & \cos(\theta + \theta_0) \end{bmatrix} \begin{bmatrix} 1 & \sin(\theta + \theta_0 + \beta) \\ 0 & \cos(\theta + \theta_0 + \beta) \end{bmatrix} \begin{Bmatrix} \xi \\ \eta \end{Bmatrix}$$
$$\begin{Bmatrix} x_{12} \\ y_{12} \end{Bmatrix} = \begin{bmatrix} \cos(\theta + \theta_0) & \sin\beta \\ \sin(\theta + \theta_0) & \cos\beta \end{bmatrix} \begin{Bmatrix} \xi \\ \eta \end{Bmatrix} \tag{8}$$

Substitution of Eq. (7) into (8) leads to

$$\begin{Bmatrix} x_{12} \\ y_{12} \end{Bmatrix} = \begin{bmatrix} \cos(\theta + \theta_0) & \sin\beta \\ \sin(\theta + \theta_0) & \cos\beta \end{bmatrix} \frac{1}{\cos(\theta_0 + \beta_0)} \begin{bmatrix} \cos\beta_0 & -\sin\beta_0 \\ -\sin\theta_0 & \cos\theta_0 \end{bmatrix} \begin{Bmatrix} x_{120} \\ y_{120} \end{Bmatrix}$$
$$\begin{Bmatrix} x_{12} \\ y_{12} \end{Bmatrix} = \begin{bmatrix} \cos(\theta + \theta_0)\cos\beta_0 - \sin\theta_0 \sin\beta & \cos\theta_0 \sin\beta - \sin\beta_0 \cos(\theta + \theta_0) \\ \sin(\theta + \theta_0)\cos\beta_0 - \sin\theta_0 \cos\beta & \cos\theta_0 \cos\beta - \sin\beta_0 \sin(\theta + \theta_0) \end{bmatrix} \begin{Bmatrix} x_{120} \\ y_{120} \end{Bmatrix} \tag{9}$$

Equation (9) is the mapping of positions. It gives the current coordinates of an arbitrary point as a function of its initial position. The displacements can therefore be computed:

$$u_{12m} = x_{12} - x_{120} = \{[\cos(\theta + \theta_0)\cos\beta_0 - \sin\theta_0 \sin\beta - \cos(\theta_0 + \beta_0)]x_{120} + [\cos\theta_0 \sin\beta - \sin\beta_0 \cos(\theta + \theta_0)]y_{120}\} \frac{1}{\cos(\theta_0 + \beta_0)} \tag{10}$$

$$v_{12m} = y_{12} - y_{120} = \{[\sin(\theta + \theta_0)\cos\beta_0 - \sin\theta_0 \cos\beta]x_{120} + [\cos\theta_0 \cos\beta - \sin\beta_0 \sin(\theta + \theta_0) - \cos(\theta_0 + \beta_0)]y_{120}\} \frac{1}{\cos(\theta_0 + \beta_0)} \tag{11}$$

It follows that the displacement derivatives are

$$\frac{\partial u_{12m}}{\partial x_{120}} = \frac{\cos(\theta + \theta_0)\cos\beta_0 - \sin\theta_0 \sin\beta}{\cos(\theta_0 + \beta_0)} - 1 \tag{12}$$

$$\frac{\partial v_{12m}}{\partial y_{120}} = \frac{\cos\theta_0 \cos\beta - \sin\beta_0 \sin(\theta + \theta_0)}{\cos(\theta_0 + \beta_0)} - 1 \tag{13}$$

$$\frac{\partial u_{12m}}{\partial y_{120}} = \frac{\cos\theta_0 \sin\beta - \sin\beta_0 \cos(\theta + \theta_0)}{\cos(\theta_0 + \beta_0)} \tag{14}$$

$$\frac{\partial v_{12m}}{\partial x_{120}} = \frac{\sin(\theta+\theta_0)\cos\beta_0 - \sin\theta_0\cos\beta}{\cos(\theta_0+\beta_0)} \tag{15}$$

and the linear strains in the matrix are

$$\varepsilon_{1m}^{L} = \frac{\partial u_{12m}}{\partial x_{120}} = \frac{\cos(\theta+\theta_0)\cos\beta_0 - \sin\theta_0\sin\beta}{\cos(\theta_0+\beta_0)} - 1 \tag{16}$$

$$\varepsilon_{2m}^{L} = \frac{\partial v_{12m}}{\partial y_{120}} = \frac{\cos\theta_0\cos\beta - \sin\beta_0\sin(\theta+\theta_0)}{\cos(\theta_0+\beta_0)} - 1 \tag{17}$$

$$\gamma_{12m}^{L} = \frac{\partial u_{12m}}{\partial y_{120}} + \frac{\partial v_{12m}}{\partial x_{120}} = \frac{\cos\theta_0\sin\beta - \sin\beta_0\cos(\theta+\theta_0) + \sin(\theta+\theta_0)\cos\beta_0 - \sin\theta_0\cos\beta}{\cos(\theta_0+\beta_0)} = \frac{\sin(\beta-\theta_0) + \sin(\theta+\theta_0-\beta_0)}{\cos(\theta_0+\beta_0)} \tag{18}$$

Notice that the displacement derivatives in Eqs. (12)-(15) and the linear strains in Eqs. (16)-(18) are constant within the matrix and they are all computed in terms of θ. For small angles, $\gamma_{12m}^{L} \approx \beta - \theta_0 + \theta + \theta_0 - \beta_0 = \beta - \beta_0 + \theta$, and Eqs. (1) and (2) reduce to $\beta \approx D_f(\theta + \theta_0)/t_m$ and $\beta_0 \approx D_f\theta_0/t_m$. Moreover, since $D_f/t_m = f/(1-f)$, then $\gamma_{12m}^{L} \approx \theta/(1-f)$, where f is the fiber volume fraction. This last expression is precisely the one derived in Gutkin *et al.* [22].

The angle θ may not be small, particularly when one considers the possibility of damage propagation. Therefore, the fully nonlinear strains should be used:

$$\varepsilon_{1m} = \frac{\partial u_{12m}}{\partial x_{120}} + \frac{1}{2}\left(\frac{\partial u_{12m}}{\partial x_{120}}\right)^2 + \frac{1}{2}\left(\frac{\partial v_{12m}}{\partial x_{120}}\right)^2 \tag{19}$$

$$\varepsilon_{2m} = \frac{\partial v_{12m}}{\partial y_{120}} + \frac{1}{2}\left(\frac{\partial u_{12m}}{\partial y_{120}}\right)^2 + \frac{1}{2}\left(\frac{\partial v_{12m}}{\partial y_{120}}\right)^2 \tag{20}$$

$$\gamma_{12m} = \frac{\partial u_{12m}}{\partial y_{120}} + \frac{\partial v_{12m}}{\partial x_{120}} + \frac{\partial u_{12m}}{\partial x_{120}}\frac{\partial u_{12m}}{\partial y_{120}} + \frac{\partial v_{12m}}{\partial x_{120}}\frac{\partial v_{12m}}{\partial y_{120}} \tag{21}$$

Angle θ is restricted to vary in an admissible range where lock-in has not occurred. The upper limit for θ may be determined by the condition that two consecutive fibers come in contact. According to Fig. 4, mathematically this condition is reached when $\pi/2 - \theta - \theta_0 - \beta = 0$. Substituting this condition into Eq. (1), and recalling that $D_f/t_m = f/(1-f)$, one concludes that $\tan(\theta + \theta_0) = (1-f)/f$.

The lower limit for θ may be determined, again, by condition that two consecutive fibers come in contact but for negative values of θ. According to Fig. 4, mathematically this condition is reached when $\pi/2 - \theta - \theta_0 - \beta = \pi$. Substituting this condition into Eq. (1) one concludes that $\tan(\theta + \theta_0) = (f - 1)/f$. However, negative values of θ will arise only when there is longitudinal traction and, in this case, the reasonable assumption is that $\theta + \theta_0 = 0$. Hence, in practice, it is expected that $-\theta_0 \le \theta \le \tan[(1-f)/f] - \theta_0$.

In order to perceive how the strains vary with θ realistic values can be assumed. Taking $\theta_0 = 3^o$ and $f = 0.5$ the practical range is $-3^o \le \theta \le 42^o$. Figure 3 shows the linear, nonlinear and total strains. It is clear that the nonlinear strains are very relevant and should be considered. The exception is perhaps γ_{12m} for angles up to 15°.

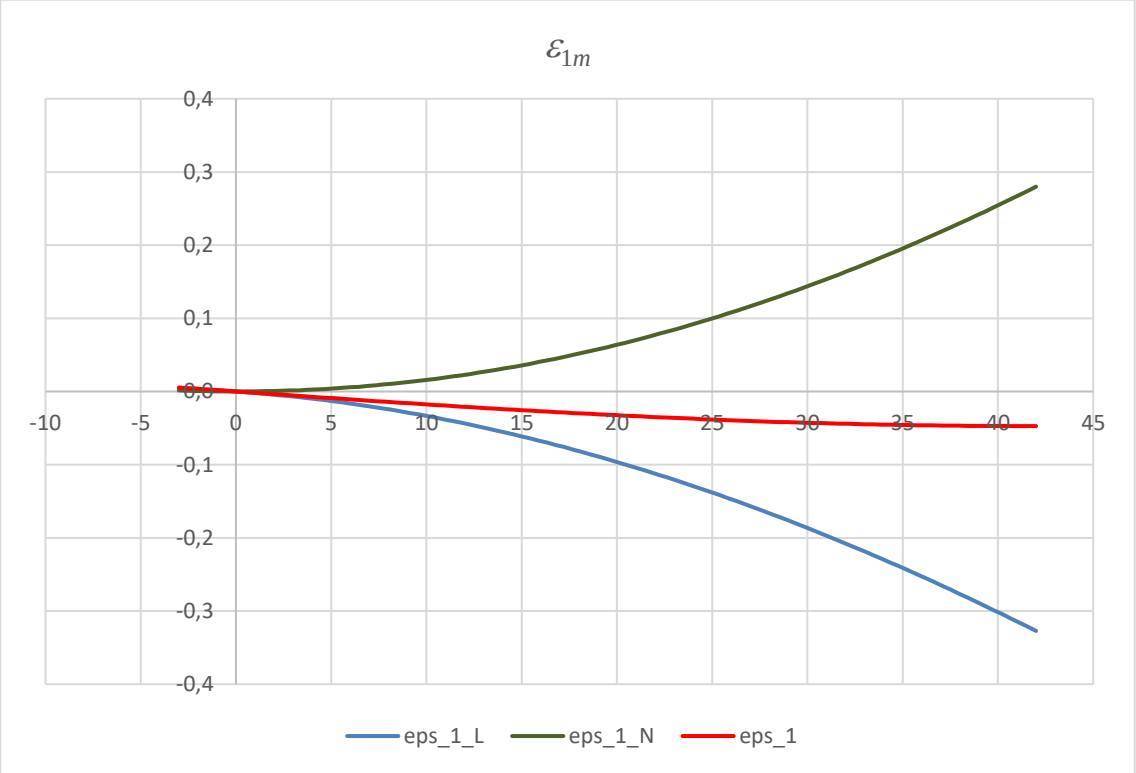
ε_{1m}
0,4
0,3
0,2
0,1
0,0
-0,1
-0,2
-0,3
-0,4
-10
-5
0
5
10
15
20
25
30
35
40
45
eps_1_L
eps_1_N
eps_1

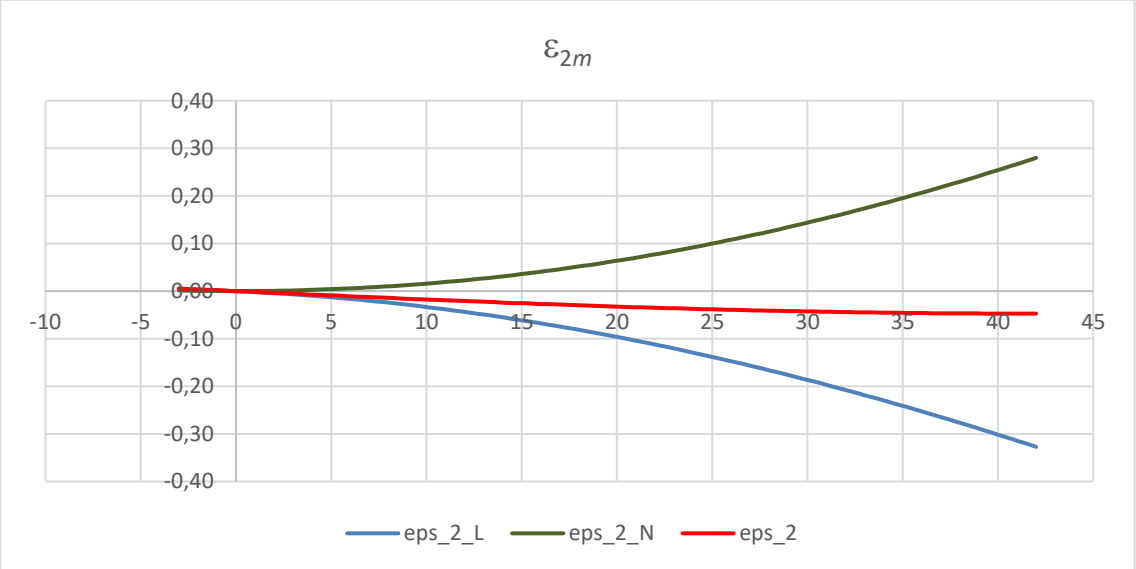
ε_{2m}
0,40
0,30
0,20
0,10
0,00
-0,10
-0,20
-0,30
-0,40
-10
-5
0
5
10
15
20
25
30
35
40
45
eps_2_L
eps_2_N
eps_2

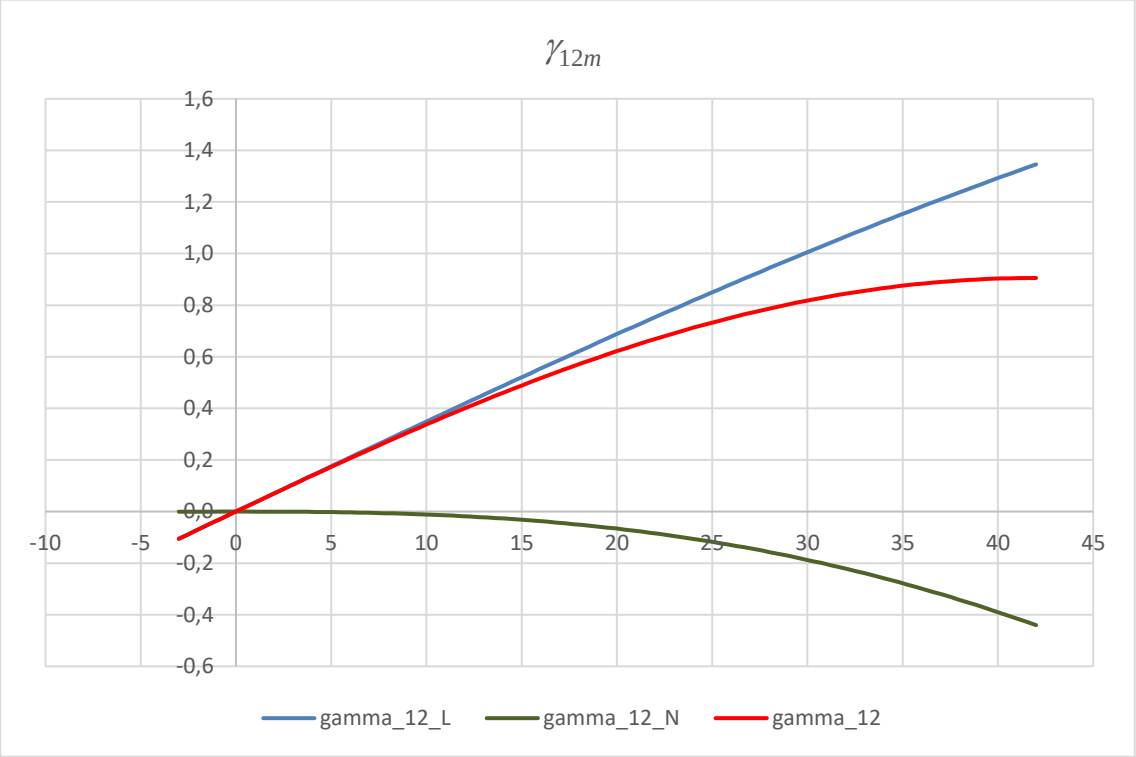

Figure 5 – Nonlinear matrix strain variations.

The methodology to compute angle θ is described next. The starting point is the consideration that the lamina homogenized strains (ε_1, ε_2, γ_{12}) in the 12 reference system are available. This is a reasonable assumption since the problem is formulated in the structural reference system XY (see Fig. 3) and strain transformations based on angle ϕ_0 are straightforward, i.e.,

$$\varepsilon_1 = \varepsilon_X \cos^2\phi_0 + \varepsilon_Y \sin^2\phi_0 + \gamma_{XY} \sin\phi_0 \cos\phi_0 \tag{22}$$

$$\varepsilon_2 = \varepsilon_X \sin^2\phi_0 + \varepsilon_Y \cos^2\phi_0 - \gamma_{XY} \sin\phi_0 \cos\phi_0 \tag{23}$$

$$\gamma_{12} = (\varepsilon_Y - \varepsilon_X)\sin(2\phi_0) + \gamma_{XY} \cos(2\phi_0) \tag{24}$$

The homogenized strains ε_1, ε_2, γ_{12} are now transformed to the reference system of misalignment xy using again Eqs. (22)-(24) with the rotation angle $\theta + \theta_0$

$$\varepsilon_x = \varepsilon_1 \cos^2(\theta+\theta_0) + \varepsilon_2 \sin^2(\theta+\theta_0) + \gamma_{12} \sin(\theta+\theta_0)\cos(\theta+\theta_0) \tag{25}$$

$$\varepsilon_y = \varepsilon_1 \sin^2(\theta+\theta_0) + \varepsilon_2 \cos^2(\theta+\theta_0) - \gamma_{12} \sin(\theta+\theta_0)\cos(\theta+\theta_0) \tag{26}$$

$$\gamma_{xy} = (\varepsilon_2 - \varepsilon_1)\sin(2\theta+2\theta_0) + \gamma_{12} \cos(2\theta+2\theta_0) \tag{27}$$

The expressions for the matrix strains obtained in Eqs. (19)-(21) with respect to the 12 reference system are also transformed to the reference system of misalignment xy.

$$\varepsilon_{xm} = \varepsilon_{1m} \cos^2(\theta+\theta_0) + \varepsilon_{2m} \sin^2(\theta+\theta_0) + \gamma_{12m} \sin(\theta+\theta_0)\cos(\theta+\theta_0) \tag{28}$$

$$\varepsilon_{ym} = \varepsilon_{1m} \sin^2(\theta+\theta_0) + \varepsilon_{2m} \cos^2(\theta+\theta_0) - \gamma_{12m} \sin(\theta+\theta_0)\cos(\theta+\theta_0) \tag{29}$$

$$\gamma_{xym} = (\varepsilon_{2m} - \varepsilon_{1m})\sin(2\theta+2\theta_0) + \gamma_{12m} \cos(2\theta+2\theta_0) \tag{30}$$

It is straightforward to see that, provided $\theta_0 = \beta_0 = 0$, Eqs. (19)-(21) reduce to $\varepsilon_{1m} = \varepsilon_{2m} = 0$ and $\gamma_{12m} = \sin(\theta+\beta)$. This goes to show that the kinematic behavior represented in Fig. 4 results chiefly in shear

strain, and consequently shear stress. From the theory of micromechanics one can write $\tau_{xym} = \tau_{xy} = \tau_{xyf}$ or $G_m\gamma_{xym} = G_{12}\gamma_{xy} = G_f\gamma_{xyf}$. The homogenized lamina shear modulus G_{12} may be computed using the classic micromechanics relation

$$\frac{1}{G_{12}} = \frac{V_f}{G_f} + \frac{1-V_f}{G_m} \tag{31}$$

Equations (27) and (30) can be used with Eqs. (12)-(15) and (19)-(21) to compute θ. Once θ is available the matrix strains ε_{1m}, ε_{2m}, γ_{12m} are calculated with the bilinear traction-separation law or the Ramberg-Osgood model. Moreover, the matrix stresses σ_{xm}, σ_{ym}, τ_{xym} can be evaluated using the constitutive relations

$$\sigma_{xm} = \frac{E_m}{1-\nu_m^2}(\varepsilon_{xm} + \nu_m\varepsilon_{ym}) \tag{32}$$

$$\sigma_{ym} = \frac{E_m}{1-\nu_m^2}(\varepsilon_{ym} + \nu_m\varepsilon_{xm}) \tag{33}$$

$$\tau_{ym} = G_m\gamma_m \tag{34}$$

The fiber strains ε_{xf}, ε_{yf}, γ_{xyf} can be evaluated using basic micromechanics

$$\varepsilon_{xf} = \varepsilon_{xm} \tag{35}$$

$$G_f\gamma_{xyf} = \tau_{xyf} = \tau_{xym} = G_m\gamma_{xym} \tag{36}$$

$$\frac{E_f}{1-\nu_f^2}(\varepsilon_{yf} + \nu_f\varepsilon_{xf}) = \sigma_{yf} = \sigma_{ym} = \frac{E_m}{1-\nu_m^2}(\varepsilon_{ym} + \nu_m\varepsilon_{xm}) \tag{37}$$

3. Application and Theoretical Validation

Figures 6 and 7a-b show a flowchart of the technique herein proposed whose intention is to help understanding the development procedure. As per Fig. 6, in addition to the fibers and resin properties, information about the Ramberg-Osgood (R&O) curve and allowable stresses are necessary in order to apply the failure criterion selected. Information on the R&O curve are referred to Travis [14].

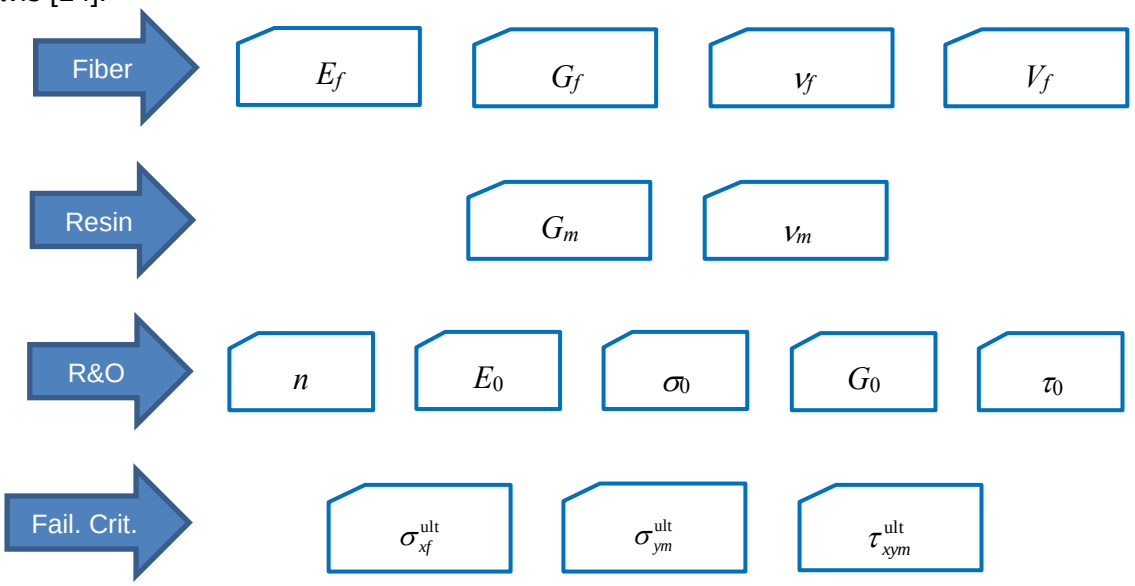

Figure 6 – Input to the calculation procedure.

In Fig. 7a one may see that the input data are relative to the laminate, i.e., the strains ε_1, ε_2 and γ_{12} and the initial misalignment θ_0. According to the flowchart in Fig. 7, as soon as convergence of the

incremental angle θ is achieved for a given load level, then, in Fig. 7b, the values of the strains and stresses in the matrix and fibers are computed for subsequent application of the selected failure criterion.

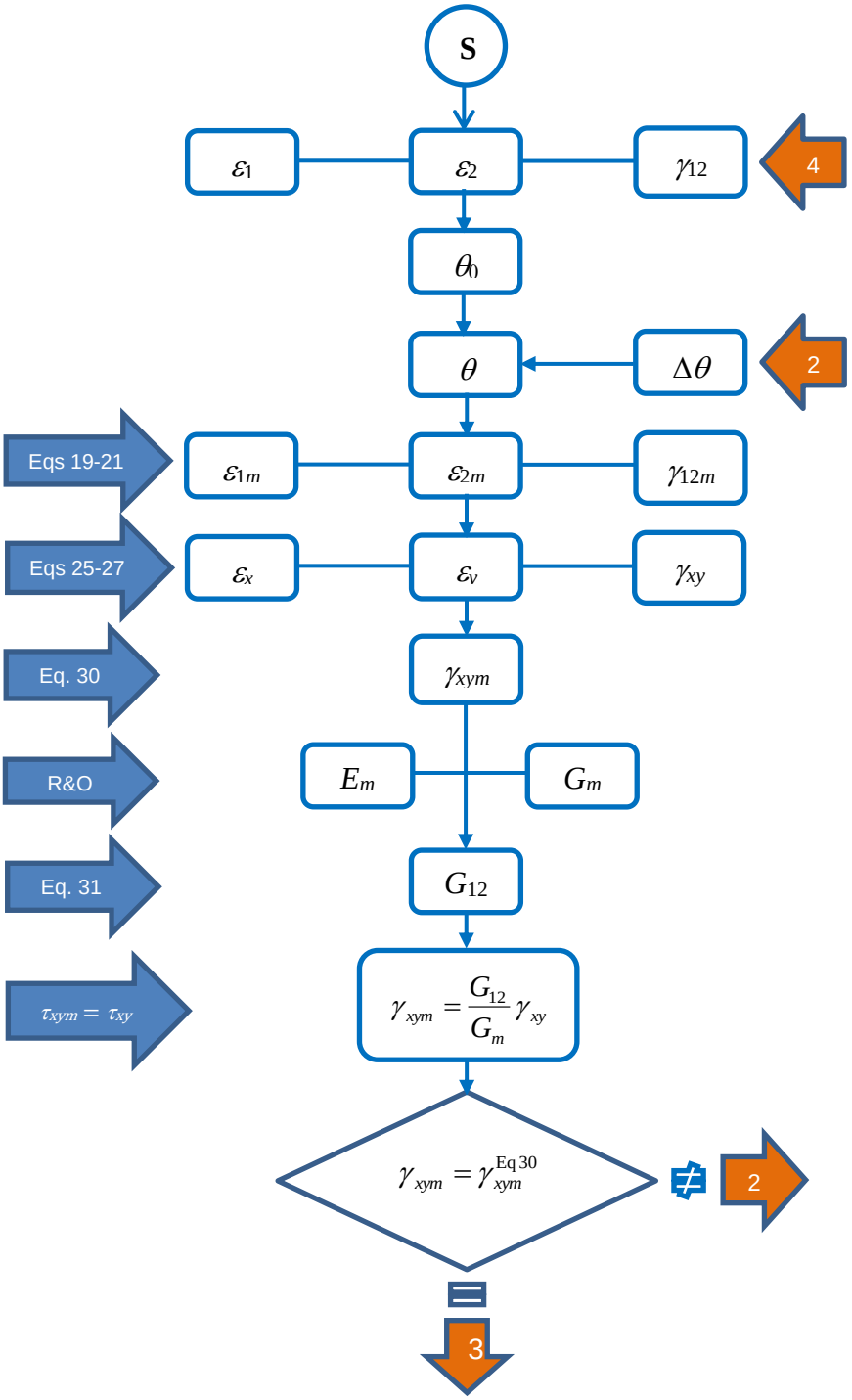

Figure 7a – Flowchart to compute θ

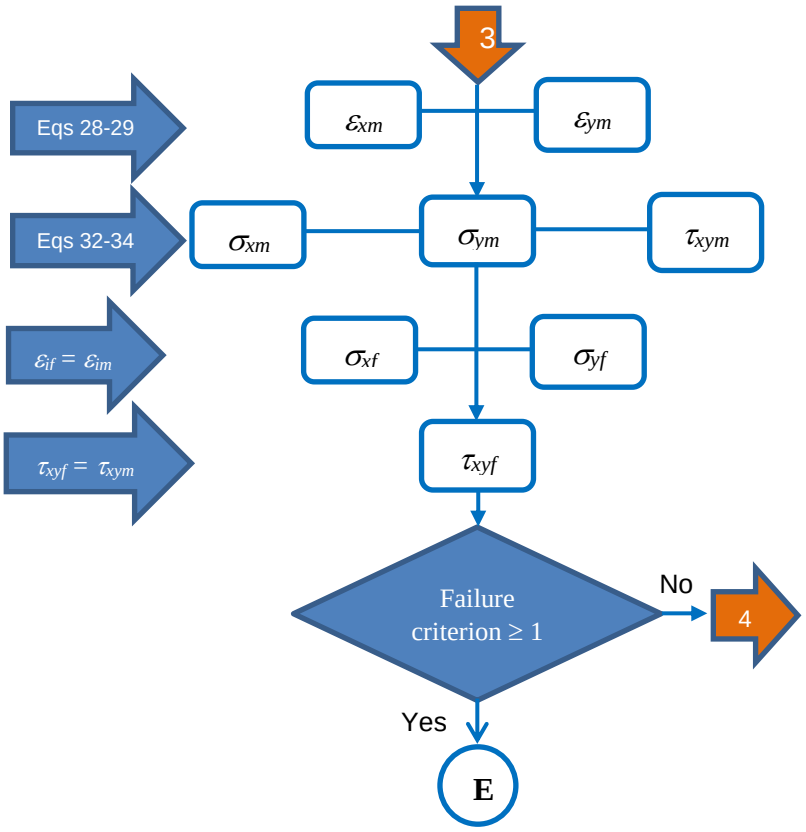

Figure 7b – Flowchart to evaluate failure criterion

In order to validate the technique the experimental results of Matsuo [18] are used. Accordingly, the dimensions of the specimen for the compression test, over the center region, are 10 mm width by 2 mm thick, and the initial misalignment θ_0 is 3º, consistent with results obtained through tridimensional X-ray reported in Matsuo [24], as illustrated in Fig. 8. The value of stress for failure under compression of the laminate with unidirectional fibers experimentally obtained was 437 MPa, at 25º C.

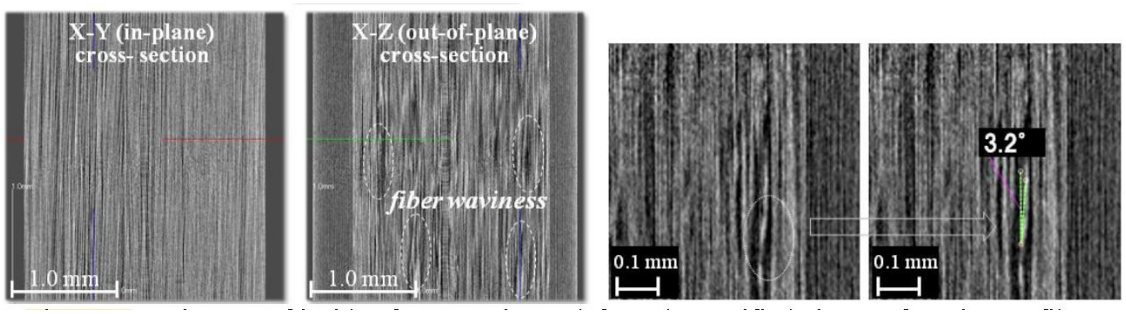

Figure 8 – Maximum initial misalignment of 3.2º [24].

In order to compare the present technique against experimental results obtained by Matsuo [18], Tab. 1 shows the values contained in Fig. 6 required for the numerical analysis.

Table 1 – Fibers, resin, R&O curve and stress allowables.

Fiber	E_f [MPa]	G_f [MPa]	ν_f	V_f	Resin	G_m [MPa]	ν_m
	10500	1520	0.59	0.50		1520	0.34
Ref.	[25]	[18]	[25]	[18]	Ref.	[18]	[19]

R&O	n	E_0 [MPa]	σ_0 [MPa]	G_0 [MPa]	τ_0 [MPa]
	3.68	105000	20.1	1520	12.5
Ref.	[18]	[25]	[18]	[18]	[18]

Hashin-Rotem	σ_{xf}^{ult} [MPa]	σ_{ym}^{ult} [MPa]	τ_{xym}^{ult} [MPa]
	437	20.1	12.5
Ref.	[18]	[18]	[18]

Determination of angle θ in the present technique begins with the knowledge of the strains ε_1, ε_2, γ_{12}. These may be obtained from laminate strains ε_x, ε_y, γ_{xy} using CLT, where the following relations are well-known:

$$\begin{Bmatrix} \mathbf{N} \\ \mathbf{M} \end{Bmatrix} = \begin{bmatrix} \mathbf{A} & \mathbf{B} \\ \mathbf{B} & \mathbf{D} \end{bmatrix} \begin{Bmatrix} \boldsymbol{\varepsilon}^0 \\ \boldsymbol{\kappa} \end{Bmatrix} \tag{38}$$

$$\begin{Bmatrix} \varepsilon_x \\ \varepsilon_y \\ \gamma_{xy} \end{Bmatrix} = \begin{Bmatrix} \varepsilon_x^0 \\ \varepsilon_y^0 \\ \gamma_{xy}^0 \end{Bmatrix} + z \begin{Bmatrix} \kappa_x \\ \kappa_y \\ \kappa_{xy} \end{Bmatrix} \tag{39}$$

$$\begin{Bmatrix} \varepsilon_1 \\ \varepsilon_2 \\ \gamma_{12} \end{Bmatrix}_k = \mathbf{T} \begin{Bmatrix} \varepsilon_x \\ \varepsilon_y \\ \gamma_{xy} \end{Bmatrix}_k \tag{40}$$

The strains ε_1, ε_2, γ_{12} in Fig. 7a are computed according to the assumptions: (a) unidirectional laminate with 15 layers (t = 2.0 mm) whose ply properties are given in Tab. 2, and (b) the load N_x, in Eq. (38), is the experimental compressive failure stress of 437 MPa, referred in Matsuo [18], and assumed load per unit thickness. As consequence, the strain values are those shown in Tab. 3.

Table 2 – Ply properties.

Ply properties	E_1 [MPa]	E_2 [MPa]	G_{12} [MPa]	ν_{12}	t_{nom} [mm]
	105000	4780	1520	0.26	0.133
Ref.	[25]	[18]	[18]	[25]	[18]

Table 3 – Strains for the ultimate compressive load.

N_x [N/mm]	ε_1	ε_2	γ_{12}
–4370	-2.0862×10^{-2}	5.4240×10^{-3}	0.0

In order to make clearer the procedure depicted in Figs. 7a-b one can, for instance, compute angle θ for half the load N_x in Tab. 3. Table 4 shows the result

Table 4 – Strains for half the load N_x.

N_x [N/mm]	ε_1	ε_2	γ_{12}
–2185	-1.0431×10^{-2}	2.7120×10^{-3}	0.0

In this case, for $\theta = 0$, the values are those presented in Tab. 5.

Table 5 – Results for half the load N_x: angle θ not converged

		Eq. 19	Eq. 20	Eq. 21	Eq. 25	Eq. 26	Eq. 27	Eq. 30	R&O	R&O	Eq. 31	$\tau_{xym} = \tau_{xy}$
θ_0	θ	ε_{1m}	ε_{2m}	γ_{12m}	ε_x	ε_y	γ_{xy}	γ_{xym}	E_m	G_m	G_{12}	γ_{xym}
deg.	deg.	[–]	[–]	[–]	$\times 10^{-3}$	$\times 10^{-3}$	$\times 10^{-3}$	[–]	MPa	MPa	MPa	$\times 10^{-3}$
3.0	0.0	0.0	0.0	0.0	–10.39	2.676	1.4	0.0	105000	1520	1520	1.4

		Eq. 28	Eq. 29	Eq. 32	Eq. 33	Eq. 34	Eq. 37	Eq. 37	Eq. 36	analysis	analysis	criterion
θ_0	θ	ε_{xm}	ε_{ym}	σ_{xm}	σ_{ym}	τ_{xym}	σ_{xf}	σ_{yf}	τ_{xyf}	fiber	matrix	R&H
[deg.]	[deg.]	[–]	[–]	[MPa]	[MPa]	[MPa]	[MPa]	[MPa]	[MPa]			F.I.
3.0	0.0	0.0	0.0	0.0	0.0	0.0	0.0	0.0	0.0	unloaded	unloaded	0.0

Observe that γ_{xym} obtained by Eq. (30) is different from γ_{xym} obtained by imposition of $\tau_{xym} = \tau_{xy}$. Thus, in the flowchart of Fig. 7a, the path to be taken is arrow "2", indicating that the value of θ must be incremented by $\Delta\theta$ in order to satisfy the equality. One may also observe in Tab. 5 that both fibers and matrix are unloaded since this is not the true situation because θ is not converged.
On the other hand, the value of θ that satisfies the condition shown in Fig. 7a, whose path is arrow "3", is shown in Tab. 6. Notice that γ_{xym} obtained by Eq. (30) is the same as γ_{xym} obtained through imposition of $\tau_{xym} = \tau_{xy}$. From Tab. 6 it can be seen that both fibers and matrix are unloaded under compression with a failure index of 0.72 according to Hashin-Rotem criterion.

Table 6 – Results for half the load N_x: angle θ converged.

		Eq. 19	Eq. 20	Eq. 21	Eq. 25	Eq. 26	Eq. 27	Eq. 30	R&O	R&O	Eq. 31	$\tau_{xym} = \tau_{xy}$
θ_0	θ	ε_{1m}	ε_{2m}	γ_{12m}	ε_x	ε_y	γ_{xy}	γ_{xym}	E_m	G_m	G_{12}	γ_{xym}
deg.	deg.	$\times 10^{-6}$	$\times 10^{-6}$	$\times 10^{-3}$	$\times 10^{-3}$	$\times 10^{-3}$	$\times 10^{-3}$	$\times 10^{-3}$	MPa	MPa	MPa	$\times 10^{-3}$
3.0	0.0	–72.51	–72.51	1.4	–10.39	2.675	1.4	1.4	101366	1517	1520	1.4

		Eq. 28	Eq. 29	Eq. 32	Eq. 33	Eq. 34	Eq. 37	Eq. 37	Eq. 36	analysis	analysis	criterion
θ_0	θ	ε_{xm}	ε_{ym}	σ_{xm}	σ_{ym}	τ_{xym}	σ_{xf}	σ_{yf}	τ_{xyf}	fiber	matrix	R&H
deg.	deg.	$\times 10^{-6}$	$\times 10^{-6}$	MPa	MPa	MPa	MPa	MPa	MPa			F.I.
3.0	0.0	0.9519	–146.0	–5.58	–16.69	2.09	–13.72	–23.42	2.09	(–)	(–)	0.72

The full load N_x of Tab. 3 corresponds to failure. In this case, for $\theta = 0$, the values computed are those presented in Tab. 7.

Table 7 – Results for full load N_x: angle θ not converged.

		Eq. 19	Eq. 20	Eq. 21	Eq. 25	Eq. 26	Eq. 27	Eq. 30	R&O	R&O	Eq. 31	$\tau_{xym} = \tau_{xy}$
θ_0	θ	ε_{1m}	ε_{2m}	γ_{12m}	ε_x	ε_y	γ_{xy}	γ_{xym}	E_m	G_m	G_{12}	γ_{xym}
deg.	deg.	[–]	[–]	[–]	$\times 10^{-3}$	$\times 10^{-3}$	$\times 10^{-3}$	[–]	MPa	MPa	MPa	$\times 10^{-3}$
3.0	0.0	0.0	0.0	0.0	–20.79	5.352	2.7	0.0	105000	1520	1520	2.7

		Eq. 28	Eq. 29	Eq. 32	Eq. 33	Eq. 34	Eq. 37	Eq. 37	Eq. 36	analysis	analysis	criterion
θ_0	θ	ε_{xm}	ε_{ym}	σ_{xm}	σ_{ym}	τ_{xym}	σ_{xf}	σ_{yf}	τ_{xyf}	fiber	matrix	R&H
[deg.]	[deg.]	[–]	[–]	[MPa]	[MPa]	[MPa]	[MPa]	[MPa]	[MPa]			F.I.
3.0	0.0	0.0	0.0	0.0	0.0	0.0	0.0	0.0	0.0	unloaded	unloaded	0.0

The results for failure condition, presented in Matsuo [18] with $\theta_0 = 3^o$, are shown in Tab. 8, along with the value of θ that satisfies the condition of the flowchart in Fig. 7a and accompanying stresses and strains.

Table 8 – Results for full load N_x: angle θ converged.

		Eq. 19	Eq. 20	Eq. 21	Eq. 25	Eq. 26	Eq. 27	Eq. 30	R&O	R&O	Eq. 31	$\tau_{xym} = \tau_{xy}$
θ_0	θ	ε_{1m}	ε_{2m}	γ_{12m}	ε_x	ε_y	γ_{xy}	γ_{xym}	E_m	G_m	G_{12}	γ_{xym}
deg.	deg.	$\times 10^{-4}$	$\times 10^{-4}$	$\times 10^{-3}$	$\times 10^{-3}$	$\times 10^{-3}$	$\times 10^{-3}$	$\times 10^{-3}$	MPa	MPa	MPa	$\times 10^{-3}$
3.0	0.08	–1.482	–1.482	2.835	–20.79	5.348	2.8	2.8	69106	1482	1520	2.8

		Eq. 28	Eq. 29	Eq. 32	Eq. 33	Eq. 34	Eq. 37	Eq. 37	Eq. 36	analysis	analysis	criterion
θ_0	θ	ε_{xm}	ε_{ym}	σ_{xm}	σ_{ym}	τ_{xym}	σ_{xf}	σ_{yf}	τ_{xyf}	fiber	matrix	R&H
deg.	deg.	$\times 10^{-6}$	$\times 10^{-6}$	MPa	MPa	MPa	MPa	MPa	MPa			F.I.
3.0	0.08	3.974	–300.3	–7.67	–23.36	4.18	–27.90	–47.99	4.18	(–)	(–)	1.46

Considering that the matrix is under compression, as observed in Tab. 8, application of the Hashin-Rotem failure criterion yields

$$\left(\frac{\sigma_2}{\sigma_{2c}^{\text{ult}}}\right)^2+\left(\frac{\tau_{12}}{\tau_{12}^{\text{ult}}}\right)^2=1 \quad \Rightarrow \quad \left(\frac{-23.36}{20.1}\right)^2+\left(\frac{4.18}{12.5}\right)^2=1.46$$

where the allowable stresses of 20.1 MPa and 12.5 MPa are reported in Tab. 1. Notice that the term responsible for failure is due to matrix compression and that the final compressive stress value used is 20.1 MPa. This value corresponds to the matrix failure stress under traction according to Matsuo [18]. Since the matrix compressive stress is higher than the matrix traction stress, the real value of the failure index must be lower than the one (1.46) just computed using the Hashin-Rotem criterion. An estimation of this real value can be made based in the work of Chao Zhao *et al.* [26]. In their work, the properties of the epoxy resin EPR-L20 were experimentally measured, and the values of strength under traction and compression are respectively 56.2 MPa and 99.1 MPa. Hence, based on these values, it is reasonable to assume that the compressive stress value for the resin might be 35.44 MPa, which is calculated assuming the simple proportional relationship 20.1 × 56.2 / 99.1 = 35.44. Therefore,

$$\left(\frac{-23.36}{35.44}\right)^2+\left(\frac{4.18}{12.5}\right)^2=0.54$$

4. Comments and Conclusions

This work proposes a technique to investigate longitudinal failure under compression in laminates with initial fiber misalignment. Despite using micromechanics as other works developed did, the greatest innovation here is the use of one single variable (increment of angle θ) to determine the problem solution.

As a partial validation, comparison against the experimental work of Matsuo [18] proved to be encouraging. It is important to highlight that the results could have been improved provided the true resin and fiber mechanical properties were available. The values of failure index computed would possibly be in the range 0.54 to 1.46. Another point to be underlined is that the final angle of approximately 3.1° adheres well to the value shown in Fig. 8.

As future work, a finite element model will be implemented to predict strains in laminates with initial misalignment, as opposed to the strains obtained by CLT where a laminate without initial misalignment is considered. Another significant step forward is the extension to 3D cases where two sequential rotations are involved in order to determine initial fiber misalignment.

5. Contact Author Email Address

Author email address arfaria@ccm-ita.org.br

6. Copyright Statement

References

[1] Tsai SW, Wu EM. A general theory of strength for anisotropic materials. *Journal of Composite Materials*, Vol .5, pp 58-80, 1971.

[2] Hashin Z, Rotem A. A fatigue failure criterion for fibre reinforced materials. *Journal of Composite*

Materials, Vol. 7, pp 448-464, 1973.

[3] Dávila CG, Camanho PP, Rose CA. Failure criteria for FRP laminates. *Journal of Composite Materials*, Vol. 39, No. 4, pp 323-345, 2005.

[4] Federal Aviation Administration. *CFR Part 25 airworthiness standards: transport category airplanes*, § 25.305 Strength and deformation. April 1970.

[5] Rosen VW. *Mechanics of composite strengthening: fibre composite materials*. Metals Park, OH: American Society of Materials, 1965.

[6] Argon AS. *Fracture of composites, treatise on materials science and technology*. New York: Academy Press, 1972.

[7] Budiansky B. Micromechanics. *Computers & Structures*, Vol. 16, No. 1-4, pp 3-12, 1983.

[8] Budiansky B, Fleck NA. Compressive failure of fibre composite. *Journal of the Mechanics and Physics of Solids*, Vol. 4, No. 1, pp 183-211, 1993.

[9] Wilhelmsson D, Talreja R, Gutkin R, Asp LE. Compressive strength assessment of fibre composites based on a defect severity model. *Composites Science and Technology*, Vol. 181, No. 8, 107685, 2019.

[10] Pimenta S, Gutkin R, Pinho ST, Robinson P. A micromechanical model for kink band formation: part II – analytical modelling. *Composites Science and Technology*, Vol. 69, No. 7-8, pp 956-964, 2009.

[11] Vogler TJ, Kyriakides S. On the initiation and growth of kink bands in fiber composites: Part I. experiments. *International Journal of Solids and Structures*, Vol. 38, No. 15, pp 2639-2651, 2001.

[12] Lee SH, Waas AM. Compressive response and failure of fiber reinforced unidirectional composites. *International Journal of Fracture*, Vol. 100, No. 3, pp 275-306, 1999.

[13] Vogler TJ, Hsu S-Y, Kyriakides S. On the initiation and growth of kink bands in fiber composites. Part II: analysis. *International Journal of Solids and Structures*, Vol. 38, No. 15, pp. 2653-2682, 2001.

[14] Bogetti TA, Staniszewski J, Burns BP, Hoppel CPR, Gillespie Jr JW, Tierney J. Predicting the nonlinear response and progressive failure of composite laminates under tri-axial loading. *Journal of Composite Materials*, Vol. 46, No. 19-20, pp 2443-2459, 2012.

[15] Chou PC, Carleone J, Hsu CM. Elastic constants of layered media. *Journal of Composite Materials*. Vol. 6, No. 1, pp 80–93, 1972.

[16] Bogetti TA, Hoppel CPR, Drysdale WH. Three-dimensional effective property and strength prediction of thick laminated composite media. ARL-TR-911, U.S. Army Research Laboratory, Aberdeen Proving Ground, MD, October 1995.

[17] Richard RM, Blacklock JR. *Finite element analysis of inelastic structures*. *AIAA Journal*, Vol. 7, No. 3, pp 432–438, 1969.

[18] Matsuo T, Kageyama, K. Compressive failure mechanism and strength of unidirectional thermoplastic composites based on modified kink band model. *Composites: Part A*, Vol. 93, pp 117-125, 2017.

[19] Vignoli LL, Savi MA, Pacheco PMCL, Kalamkarov AL. Micromechanical analysis of longitudinal and shear strength of composite laminae. *Journal of Composite Materials*, Vol. 54, No. 30, pp 4853-4873, 2020.

[20] Zhang D, Waas AM. A micromechanics based multiscale model for nonlinear composites. Acta Mechanica, Vol. 225, pp 1391-1417, 2014.

[21] Huang ZM. Micromechanical prediction of ultimate strength of transversely isotropic fibrous composites. *International Journal of Solids and Structures*, Vol. 38, No. 22-23, pp 4147-4172, 2001.

[22] Gutkin R, Pinho ST, Robinson P, Curtis PT. A finite fracture mechanics formulation to predict fibre kinking and splitting in CFRP under combined longitudinal compression and in-plane shear. *Mechanics of Materials*, Vol. 43, No. 11, pp 730-739, 2011.

[23] Ramberg W, Osgood WR. Description of stress-strain curves by three parameters. Technical Note No. 902, National Advisory Committee for Aeronautics, Washington DC, 1943.

[24] Matsuo T, Kageyama K. Investigation about temperature dependence of unidirectional compressive strength of carbon fiber reinforced thermoplastic composites. *Proceedings of ICCM-20 Conference*. Copenhagen, July 2015.

[25] Matsuo T, Kageyama K. Design and manufacture of anisotropic hollow beam using thermoplastic composites. *Proceeding of the 19th International Conference on Composite Materials*, Montreal, 28th July - 2nd August 2013.

[26] Zhao C, Huang Y, Chen Z, Ha SK. Progressive failure prediction of a landing gear structure of braided composites. *Composite Structures*, Vol. 161, No. 1, pp 407-418, 2017.